J|A|C|S
ARTICLES
Published on Web 05/01/2007

A Cu/Pt Near-Surface Alloy for Water−Gas Shift Catalysis

Jan Knudsen,[†] Anand U. Nilekar,[‡] Ronnie T. Vang,[†] Joachim Schnadt,[†] Edward L. Kunkes,[‡] James A. Dumesic,[‡] Manos Mavrikakis,*[,‡] and Flemming Besenbacher*[,†]

Contribution from the Interdisciplinary Nanoscience Center (iNANO) and Department of Physics and Astronomy, University of Aarhus, DK-8000 Aarhus C, Denmark, and Department of Chemical and Biological Engineering, University of Wisconsin−Madison, Madison, Wisconsin 53706

Received January 5, 2007; E-mail: manos@engr.wisc.edu; fbe@inano.dk

Abstract: The primary route to hydrogen production from fossil fuels involves the water−gas shift (WGS) reaction, and an improvement in the efficiency of WGS catalysts could therefore lead to a major leap forward in the realization of hydrogen economy. On the basis of a combination of high-resolution scanning tunneling microscopy, X-ray photoelectron spectroscopy, and density functional theory (DFT) calculations, we suggest the existence of a new thermodynamically stable Cu/Pt near-surface alloy (NSA). Temperature-programmed desorption and DFT reveal that this Cu/Pt NSA binds CO significantly more weakly than does Pt alone, thereby implying a considerable reduction in the potential for CO poisoning of the Cu/Pt NSA surface as compared to that of pure Pt. In addition, DFT calculations show that this Cu/Pt NSA is able to activate H_2O easily, which is the rate-determining step for the WGS on several metal surfaces, and, at the same time, to bind the products of that reaction and formate intermediates rather weakly, thus avoiding possible poisoning of the catalyst surface. The Cu/Pt NSA is thus a promising candidate for an improved WGS catalyst.

1. Introduction

The water−gas shift (WGS) reaction, in which carbon monoxide (CO) reacts with water (H_2O) to form carbon dioxide (CO_2) and hydrogen (H_2),[1] is used extensively in the conversion of fossil fuel to hydrogen. In particular, WGS removes residual CO from reformate hydrogen gas, which is important when hydrogen is used as a fuel for low-temperature fuel cells; the performance of such fuel cells is very sensitive to CO impurities because of CO poisoning of the Pt-based anode.[2−4]

The WGS reaction is slightly exothermic (∼40 kJ/mol), and therefore low reaction temperatures push the equilibrium toward hydrogen production, while high reaction temperatures provide faster kinetics. To deal with these two opposing temperature effects, large-scale industrial plants often use a two-step WGS reactor in which the feed gas is led through a high-temperature WGS reactor and then a low-temperature recator.[5] However, such a two-step process is not a viable solution for small-scale applications such as on-board reformers in hydrogen fuel cell-powered automobiles. Consequently, it is very important to develop new WGS catalysts with high activity at lower temperatures than the presently used low-temperature Cu-based WGS catalysts.

Transition metal alloys are very often superior to pure transition metals as the active materials in heterogeneous catalysis.[6] During the past century, the development of alloy catalysts has almost exclusively been accomplished by trial and error. Recent advances in both experimental and theoretical methods, however, have facilitated the development of new and improved alloy catalysts based on fundamental surface science and first-principles studies.[7−10] These advances continue to pave the way for a new era in which promising catalysts may be identified directly from first principles.[8,11−13]

Here, we report on a novel Cu/Pt near-surface alloy (NSA) with an enhanced Cu concentration in the first subsurface layer of the Pt host, which is shown to be a promising candidate for an improved low-temperature WGS catalyst. From an interplay of scanning tunneling microscopy (STM), X-ray photoelectron

[†] University of Aarhus.
[‡] University of Wisconsin−Madison.

(1) Ovesen, C. V.; Stoltze, P.; Norskov, J. K.; Campbell, C. T. *J. Catal.* **1992**, *134*, 445−468.
(2) *Handbook of Fuel Cells: Fundamentals, Technology, Applications*; Wiley: West Sussex, UK, 2003.
(3) Oetjen, H. F.; Schmidt, V. M.; Stimming, U.; Trila, F. *J. Electrochem. Soc.* **1996**, *143*, 3838−3842.
(4) Greeley, J.; Mavrikakis, M. *Catal. Today* **2006**, *111*, 52−58.
(5) Somorjai, G. *Introduction to Surface Chemistry and Catalysis*; John Wiley & Sons: New York, 1994.
(6) Sinfelt, J. *Bimetallic Catalysts: Discoveries, Concepts and Applications*; Wiley: New York, 1983.
(7) Besenbacher, F.; Chorkendorff, I.; Clausen, B. S.; Hammer, B.; Molenbroek, A. M.; Norskov, J. K.; Stensgaard, I. *Science* **1998**, *279*, 1913−1915.
(8) Greeley, J.; Mavrikakis, M. *Nat. Mater.* **2004**, *3*, 810−815.
(9) Vang, R. T.; Honkala, K.; Dahl, S.; Vestergaard, E. K.; Schnadt, J.; Laegsgaard, E.; Clausen, B. S.; Norskov, J. K.; Besenbacher, F. *Nat. Mater.* **2005**, *4*, 160−162.
(10) Jacobsen, C. J. H.; Dahl, S.; Clausen, B. S.; Bahn, S.; Logadottir, A.; Norskov, J. K. *J. Am. Chem. Soc.* **2001**, *123*, 8404−8405.
(11) Zhang, J. L.; Vukmirovic, M. B.; Xu, Y.; Mavrikakis, M.; Adzic, R. R. *Angew. Chem., Int. Ed.* **2005**, *44*, 2132−2135.
(12) Zhang, J. L.; Vukmirovic, M. B.; Sasaki, K.; Nilekar, A. U.; Mavrikakis, M.; Adzic, R. R. *J. Am. Chem. Soc.* **2005**, *127*, 12480−12481.
(13) Greeley, J.; Jaramillo, T. F.; Bonde, J.; Chorkendorff, I. B.; Norskov, J. K. *Nat. Mater.* **2006**, *5*, 909−913.

spectroscopy (XPS), and density functional theory (DFT) calculations, we show that a thermodynamically stable Cu/Pt NSA, with Cu preferentially located in the first subsurface layer, is formed upon evaporation of 1 monolayer (ML) of Cu onto Pt(111) at 800 K. Temperature-programmed desorption (TPD) and DFT studies show that the potential for CO poisoning of the Cu/Pt NSA is reduced compared to that of pure Pt. Finally, we use DFT to analyze trends in catalytic activation of water, which is the rate-determining step for the WGS on several metal surfaces, and the binding of formate, a common spectator species that blocks sites on Cu WGS catalysts. By combining these results, we propose that the Cu/Pt(111) NSA possesses a higher WGS activity than the pure Cu(111) surface of the industrially used WGS catalyst.

2. Methods

The STM experiments were performed in an ultra-high-vacuum system with a base pressure of $\sim 10^{-10}$ Torr, equipped with the home-built Aarhus STM.[14] A Pt(111) crystal was cleaned with cycles of Ar ion sputtering (1.0 keV, 10 min) followed by annealing to 1000 K for 3 min. These cycles were repeated until no contamination of the crystal could be detected with the STM. Cu was deposited either by a home-built evaporator consisting of a piece of Cu placed in a resistively heated tungsten crucible or with a mini e-beam evaporator (Oxford Applied Research). Both evaporators were calibrated from STM pictures of Cu evaporated onto Pt(111) at room temperature. All XPS measurements of Cu 3s were performed at the SX700 beamline located at the Aarhus Storage Ring in Denmark (ASTRID), with $h\nu = 205$ eV in normal emission. A fixed 100 mm mean radius analyzer (VG-CLAM2) was used in all experiments. The TPD measurements were obtained using a Balzers quadrupole mass spectrometer, after the crystal was exposed to 10 L of CO at 166 K, and with a heating rate of 2 K/s.

The self-consistent DFT calculations were carried out using the DACAPO[15,16] total-energy code with ultrasoft pseudopotentials, plane waves with kinetic energies of up to 25 Ry, and 6 or 18 *k*-points in the first Brillouin zone for (111) facets of four-layer metal slabs with 3×3 and 2×2 surface unit cells, respectively. The equivalent of five layers of vacuum was used to separate periodic images of metal slabs in the *z*-direction of the unit cell. Adsorption is allowed on only one of the two exposed surfaces, and the electrostatic potential is adjusted accordingly.[17,18] All CO and formate (HCOO) binding energy calculations were performed at a coverage of 1/9 ML on a 3×3 surface unit cell, whereas a 2×2 unit cell was used for the calculation of the activation energy barrier for H_2O dissociation. Ionic cores were described by ultrasoft pseudopotentials,[19] and the Kohn−Sham one-electron valence states were expanded in a basis of plane waves with kinetic energy below 25 Ry. The exchange-correlation energy and potential were described self-consistently within the generalized gradient approximation (GGA-PW91).[20,21] The self-consistent PW91 density was determined by iterative diagonalization of the Kohn−Sham Hamiltonian, Fermi population of the Kohn−Sham states ($k_BT = 0.1$ eV), and Pulay mixing of the resulting electronic density.[22] All total energies have been extrapolated to $k_BT = 0$ eV. Zero-point energy effects were not considered in the reported results. Unless otherwise specified, all degrees of freedom for the top two layers of slab atoms and for all adsorbate atoms were relaxed. Transition states for H_2O dissociation were located with the "climbing-image nudged elastic band" method.[23]

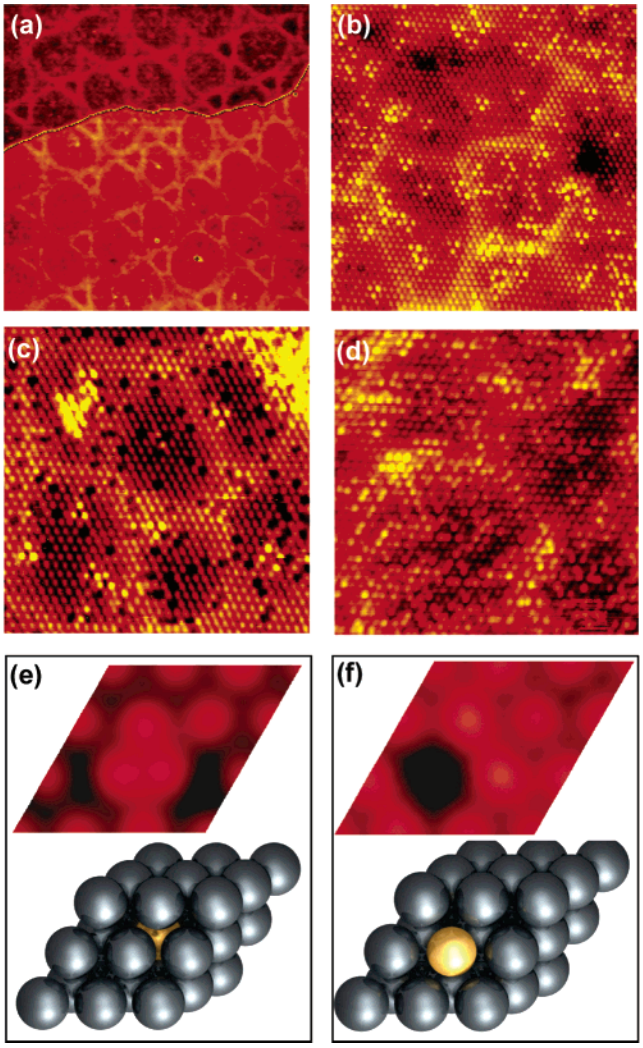

Figure 1. (a−d) STM images of Cu/Pt(111) surface alloys. (a,b) Surface prepared by evaporation of 1 ML of Cu onto Pt(111) at 800 K (image sizes are 631×631 Å^2 and 132×132 Å^2, respectively). (c) Surface prepared by the evaporation of 1 ML of Cu onto Pt(111) followed by 1 ML of Pt at room temperature (100×100 Å^2). (d) The surface in (c) after postannealing at 773 K (100×100 Å^2). (e,f) Simulated STM images of a Cu atom (gold spheres) in the first subsurface layer (e) or in the topmost layer (f) of a Pt(111) substrate (gray spheres) within the framework of a 3×3 surface unit cell.

3. Results and Discussion

When Cu was evaporated onto a Pt(111) crystal, the STM images clearly indicated the formation of an NSA.[8] In particular, Figure 1a shows an STM image of a Pt(111) surface after evaporation of 1 ML of Cu at a substrate temperature of 800 K. The surface displays a network of bright rings ordered in a nonperfect hexagonal symmetry with a periodicity of ~100 Å. These bright lines are speculated to be stress-induced boundaries between atoms sitting in face-centered cubic (fcc) and hexagonal close-packed (hcp) sites.[24,25] Atomically resolved images (Figure

(14) Laegsgaard, E.; Besenbacher, F.; Mortensen, K.; Stensgaard, I. *J. Microsc. (Oxford)* **1988**, *152*, 663−669.
(15) Hammer, B.; Hansen, L. B.; Nørskov, J. K. *Phys. Rev. B* **1999**, *59*, 7413−7421.
(16) Greeley, J.; Nørskov, J. K.; Mavrikakis, M. *Annu. Rev. Phys. Chem.* **2002**, *53*, 319−348.
(17) Neugebauer, J.; Scheffler, M. *Phys. Rev. B* **1992**, *46*, 16067−16080.
(18) Bengtsson, L. *Phys. Rev. B* **1999**, *59*, 12301−12304.
(19) Vanderbilt, D. *Phys. Rev. B* **1990**, *41*, 7892−7895.
(20) Perdew, J. P.; Chevary, J. A.; Vosko, S. H.; Jackson, K. A.; Pederson, M. R.; Singh, D. J.; Fiolhais, C. *Phys. Rev. B* **1992**, *46*, 6671−6687.
(21) White, J. A.; Bird, D. M. *Phys. Rev. B* **1994**, *50*, 4954−4957.
(22) Kresse, G.; Furthmuller, J. *Comput. Mater. Sci.* **1996**, *6*, 15−50.
(23) Henkelman, G.; Jónsson, H. *J. Chem. Phys.* **2000**, *113*, 9978−9985.
(24) Holst, B.; Nohlen, M.; Wandelt, K.; Allison, W. *Surf. Sci.* **1997**, *377*, 891−894.
(25) Holst, B.; Nohlen, M.; Wandelt, K.; Allison, W. *Phys. Rev. B* **1998**, *58*, R10195−R10198.

1b) reveal that the surface atoms appear with different corrugations in the STM images, which serves as a clear indication of NSA formation. In the topmost surface layer, we did not find any dislocations visible to the STM. Therefore, we conclude that the bright lines observed in the STM images are related to subsurface atoms changing between stacking of fcc and hcp sites.

A ring structure very similar to the one described above was observed when we evaporated 1 ML of Cu onto Pt(111), followed by evaporation of 1 ML of Pt at room temperature, where both Cu and Pt grow as adlayers. As can be seen in Figure 1c, similar bright lines show up in the STM images of this "sandwich" structure. However, some atoms in the topmost layer are imaged as depressions, which we did not observe in the original ring structure. These dark spots disappear upon annealing to 773 K (Figure 1d), in which case we end up with a structure almost identical to the ring structure of Figure 1b.

The wave functions derived from DFT calculations were used to calculate STM images[26] by employing the Tersoff−Hamann approach.[27] These calculations were performed for a number of configurations with Cu located on the surface and/or subsurface of Pt(111). The simulated STM image shown in Figure 1e represents a single Cu atom in the second layer of the Pt(111) slab; this image is in qualitatively good agreement with the trimers of bright atoms observed by STM between the rings in Figure 1b. The simulated STM image of a surface Cu atom in a Pt(111) substrate (Figure 1f) shows a distinct depression, which strongly suggests that the dark spots in the sandwich structure are Cu atoms incorporated in the topmost layer. These depressions are not observed in the ring structure, and we therefore conclude that evaporation of 1 ML of Cu onto Pt(111) at 800 K leads to the formation of NSA without Cu atoms in the surface layer.

To further investigate the formation of the subsurface Cu/Pt alloy, we used DFT calculations to determine the thermodynamics and energetic aspects of its formation kinetics. From calculations on a 3×3 surface unit cell of a seven-layer Pt(111) slab, we found that the activation energy barrier for both Pt vacancy formation in Pt(111) and Cu adatom diffusion from the surface of Pt(111) into a Pt vacancy in Pt(111) is less than 3 eV. Barriers of this magnitude can be surmounted at 800 K, the sample temperature during the original Cu deposition, and thus we expect a structure in thermodynamic equilibrium. We analyzed the relative stability of Cu atoms in various layers of the seven-layer Pt(111) slab, now allowing for relaxation of the top five layers. By replacing one or two of the Pt atoms in the slab with Cu atoms, either in the top (i.e., surface) layer or in the second, third, or fourth layer of the slab, we were able to determine the relative energetics as a function of Cu coverage (1/4 or 1/2 ML, respectively). We found that 1/4 ML of Cu is more stable when located in the second, third, or fourth layer of the slab by 0.48, 0.34, or 0.35 eV, respectively, than when Cu is located in the surface layer. Furthermore, these trends in the relative energetics of Cu in Pt(111) remain practically invariant when the Cu coverage is increased to 1/2 ML or when a Pt(100) facet is considered instead of the Pt(111) facet. Studies of Cu on/in facets of Pt other than the (111) facet may be relevant to realistic catalyst nanoparticles, naturally exposing a mixture of crystallographic facets. In all cases, the relative stability of Cu in the third and fourth layers of the Pt slab appears to be converged to what we consider to be the stability of Cu in bulk Pt. These results show that a significant driving force causes Cu to diffuse into the Pt slab rather than staying in the surface layer, and that the thermodynamics of Cu−Pt alloy dictate a preferential occupation of sites within the first subsurface layer of Pt(111).

This conclusion was verified by XPS measurements, which showed a 70% attenuation of the Cu 3s peak when an overlayer of Cu on Pt(111) was flashed to 800 K, while the peak intensity was not attenuated any further when the sample was kept at 800 K for longer periods.

Finally, our DFT results for Cu on/in Pt(100) indicate trends similar to those established above for Pt(111), in terms of both the thermodynamics and kinetics of the subsurface alloy formation. If anything, the migration of Cu to the subsurface of Pt becomes even easier through the more open (100) facet.

A depth profile of Cu in the Pt(111) host can be obtained from the DFT-calculated stabilization energies of Cu in different layers and the XPS data discussed above. The Cu 3s intensity of the subsurface alloy, I, relative to the intensity of the overlayer, I_0, can be expressed as the following sum, if it is assumed that the Cu atoms are distributed in a finite number of layers, N, close to the surface:

$$\frac{I}{I_0} = \sum_{i=1}^{N} c_i \exp\left(-\frac{(i-1)d}{\mu}\right)$$

Here, c_i is the concentration of Cu in layer i, μ is the inelastic mean free path of the electron in Pt(111), and d is the interlayer distance in Pt(111) since the amount of Cu in the Pt(111) host is relatively low. The concentration of Cu atoms in the surface layer is observed to be zero in the STM, as discussed above, and c_1 is therefore equal to zero. The DFT calculations show that the relative stability of Cu converges to the bulk value in the third layer, and c_i is therefore assumed to be constant for $i \geq 3$. From a Boltzman distribution, we can determine the relative Cu concentration in the second layer (c_2) with respect to the bulk value (c_{bulk}):

$$\frac{c_2(\text{Cu})}{c_{\text{bulk}}(\text{Cu})} = \exp\left(\frac{E_2 - E_{\text{bulk}}}{kT}\right)$$

$$= \exp\left(\frac{0.48\ \text{eV} - 0.35\ \text{eV}}{(8.62 \times 10^{-5}\ \text{eV/K}) \times 800\ \text{K}}\right) = 6.6$$

Finally, the sum can be rewritten as

$$\frac{I}{I_0} = 0.30 = c_2 \exp\left(\frac{-d}{\mu}\right) + \frac{c_2}{6.6}\sum_{i=3}^{N} \exp\left(\frac{-(i-1)d}{\mu}\right)$$

This equation is solved under the constraint that the total amount of Cu is fixed to 1 ML. The best agreement with the experimentally observed damping is obtained with 0.4 ML of Cu in the second layer and 0.06 ML of Cu in layers 3−11.

Having discussed the atomic-scale structure of the Cu/Pt NSA, we now turn our attention to its WGS reactivity. First, we use DFT calculations and TPD experiments to probe the strength

(26) Bollinger, M. V.; Lauritsen, J. V.; Jacobsen, K. W.; Norskov, J. K.; Helveg, S.; Besenbacher, F. *Phys. Rev. Lett.* **2001**, *87*, 196803.
(27) Tersoff, J.; Hamann, D. R. *Phys. Rev. B* **1985**, *31*, 805−813.

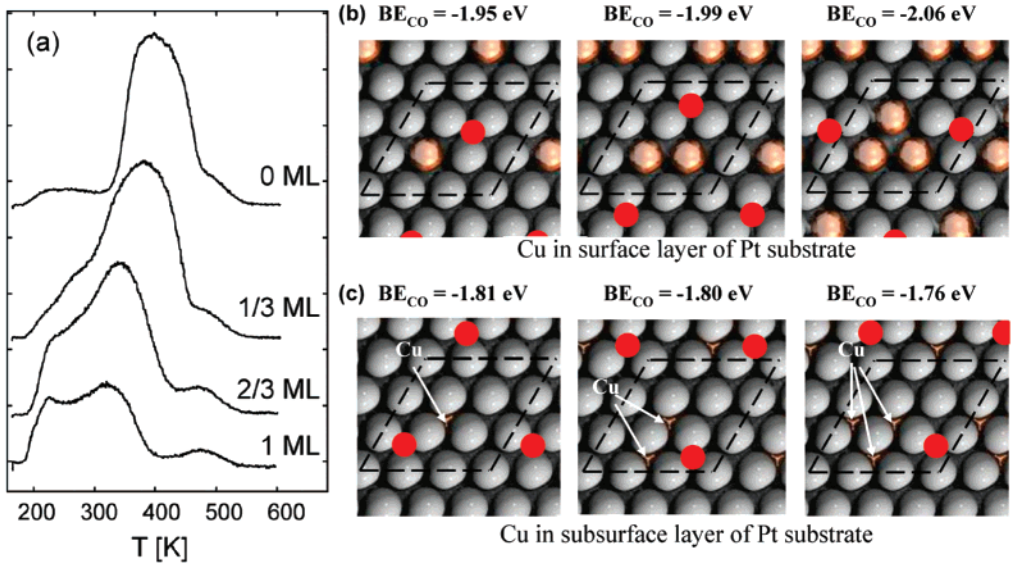

Figure 2. (a) Series of CO TPD spectra for Cu/Pt(111) surface alloys with varying amounts of Cu after exposure of 10 L of CO at 166 K. (b,c) Binding energies for 1/9 ML of CO on different Cu/Pt surface and subsurface alloys, respectively, as calculated from a 3 × 3 surface unit cell (for comparison, BE_{CO} on pure Pt(111) = −1.82 eV). Gray and gold spheres represent Pt and Cu atoms, respectively. In each of the panels (b) and (c), three top views of the respective alloy slabs are shown: left, 1/9ML of Cu; middle, 2/9 ML of Cu; right, 3/9 ML of Cu. The surface unit cell is sketched in each image, with the most favored CO adsorption site shown with a red circle. In panel (c), arrows show the location of the subsurface Cu atoms.

of the interaction between CO and the Cu/Pt NSA; the stronger the interaction, the more likely the site-blocking by CO would be. In particular, we calculated the binding energy ($E_b = E_{total} - E_{substrate} - E_{gas-phase\ adsorbate}$) of CO on pure Pt(111) and on Cu/Pt(111) NSAs with varying concentrations of Cu in the surface and subsurface layers at a CO coverage of 1/9 ML. For reference, the binding energy of CO on Pt(111) is found to be −1.82 eV. It should be noted that, although DFT methods are unable to capture the most stable CO adsorption site on Pt-(111),[28] here we focus only on the trends in CO binding energies on different surfaces, and these relative trends should not be affected by that inability. When the Cu coverage for the Cu overlayer structures was increased from 1/9 to 1/3 ML, an increase in the magnitude of the binding energy of CO in the most preferred site (fcc site formed by three Pt atoms) was calculated. The CO binding energies in these cases amount to −1.95 eV for 1/9 ML of Cu and −2.06 eV for 1/3 ML of Cu (see Figure 2b). For the Cu subsurface alloys of Pt(111), we observe exactly the opposite behavior. As the Cu concentration in the second layer of the slab is increased from 1/9 ML to 1/3 ML, the magnitude of the CO binding energy on the most preferred surface site decreases from −1.81 to −1.76 eV, as shown in Figure 2c. As the amount of Cu in the subsurface layer is further increased to 1 ML, the CO binding is decreased by 0.33 eV, to −1.48 eV. CO binding is significantly weaker on a full ML of Cu overlayer on top of Pt(111) (−1.16 eV) as compared to the different structures considered above, but it is important to remember that this structure is not thermodynamically stable because Cu is clearly more stable in subsurface layers.

The trends in CO binding energies as predicted by DFT were investigated experimentally by performing TPD measurements on various Cu/Pt(111) structures. A series of CO TPD spectra from Cu/Pt(111) subsurface alloys, prepared by evaporating varying amounts of Cu onto Pt(111) at 800 K, is depicted in Figure 2a. The TPD spectrum from the pure Pt(111) surface has a broad but distinct peak with a maximum intensity at 400 K and a small, high-temperature shoulder, which is ascribed to defects such as step edges.[29] When the amounts of Cu alloyed into Pt(111) are increased, the main TPD peak shifts toward lower temperatures, which shows that the Cu atoms weaken the interaction between the surface alloy and CO. This trend in CO binding energy as a function of Cu coverage is exactly what is found in the DFT calculations for the Cu/Pt(111) subsurface alloys, but not for the surface alloys. Therefore, the combination of DFT and TPD shows that the thermodynamically stable Cu/Pt NSA binds CO significantly more weakly than Pt(111) does, thereby implying a considerable enhancement of CO-tolerance of the Cu/Pt NSA surface as compared to that of pure Pt.

Detailed studies of the low-temperature WGS reaction mechanism on a number of late transition metals[30] suggest that H_2O activation, and in particular its first step ($H_2O \rightarrow OH + H$), is the rate-determining step for several of these metals. This includes Cu, the current catalyst of choice for industrial WGS applications,[31] and Pt. Accordingly, we have studied the minimum energy path of water activation on three different model surfaces, Cu(111), Pt(111), and a full ML of Cu in the first subsurface layer of a Pt(111) slab. As shown above, Cu preferentially segregates into the first subsurface layer of Pt(111) without necessarily reaching a full ML coverage in that layer. However, previous calculations on NSAs[8] showed that positive kinetic effects (such as decreased activation energies) observed at full ML subsurface alloys tend to be preserved by-and-large, even in the case of less than a ML of solute coverage in the subsurface layer. This finding reflects the importance of local

(28) Feibelman, P.; Hammer, B.; Nørskov, J.; Wagner, F.; Scheffler, M.; Stumpf, R.; Watwe, R.; Dumesic, J. *J. Phys. Chem. B* **2001**, *105*, 4018−4025.
(29) Pedersen, M. O.; Helveg, S.; Ruban, A.; Stensgaard, I.; Laegsgaard, E.; Norskov, J. K.; Besenbacher, F. *Surf. Sci.* **1999**, *426*, 395−409.
(30) Gokhale, A. A. Ph.D. thesis, University of Wisconsin−Madison, 2005.
(31) Chorkendorff, I.; Niemantsverdriet, J. W. *Concepts of Modern Catalysis and Kinetics*; Wiley-VCH: Weinheim, 2003.

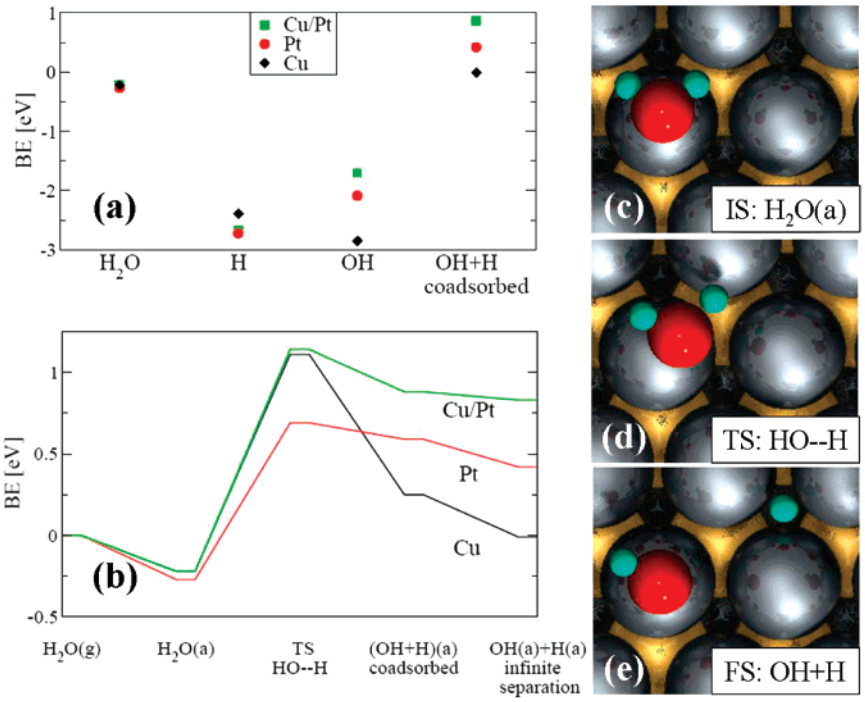

Figure 3. (a) Binding energies (BE) of H_2O (ref $H_2O(g)$), H (ref H(g)), OH (ref OH(g)), and coadsorbed OH + H (ref $H_2O(g)$) on Cu(111), Pt(111), and Cu/Pt(111), all calculated on a 2 × 2 unit cell, for the energetically preferred states. (b) Potential energy diagram for the activation of H_2O on Cu/Pt(111) subsurface alloy, Cu(111), and Pt(111) with $H_2O(g)$ as the zero of the energy axis. (c−e) Top view of DFT-calculated structures for the initial (IS), transition (TS), and final (FS) states of H_2O activation on the Cu/Pt(111) subsurface alloy. Red, green, gray, and gold spheres represent O, H, Pt, and Cu atoms, respectively.

electronic structure in determining specific site reactivity. Thus, by choosing a high-symmetry, full ML Cu/Pt subsurface alloy, we can examine the influence of subsurface Cu on the reactivity of the Pt surface.

The binding energies at their preferred adsorption sites of H, OH, and H_2O on all three surfaces are shown in Figure 3a. We find that, in the 2 × 2 unit cell, H and OH occupy three-fold fcc sites on all three surfaces, with the exception of OH occupying top/bridge site on the pure Pt(111) surface. In the relevant coadsorbed states, representing the final state of H_2O activation, OH and H occupy top−fcc, fcc−fcc, and top−top combinations of sites on Cu/Pt(111), Cu(111), and Pt(111), respectively. The variation in the binding energy of H on these three surfaces is small (within 0.20 eV) as compared to the corresponding variation of the OH binding energy (1.15 eV). OH binds to Cu/Pt(111) with −1.70 eV, significantly weaker than on Cu(111) and Pt(111), to which it binds with −2.85 and −2.09 eV, respectively. H_2O interacts rather weakly with all three surfaces.

Following the trend in relative stability of adsorbed OH discussed above, the coadsorbed state of the products for the $H_2O \rightarrow OH + H$ step is most stable on Cu(111), followed by Pt(111) and then by Cu/Pt(111). A significant repulsion between coadsorbed OH and H calculated on the Cu(111) surface tends to stabilize the products of this reaction even further when OH and H can diffuse away from each other (compare the coadsorbed state and infinite separation state, as shown in Figure 3b). However, this is not the case on the other two surfaces, where the repulsive interaction between coadsorbed OH and H is only minimal. Figure 3b shows that the activation energy barrier for the $H_2O \rightarrow OH + H$ elementary step is the smallest on Pt(111), a modest 0.96 eV, whereas the corresponding barriers on Cu(111) and Cu/Pt(111) subsurface alloy are 1.34 and 1.36 eV, respectively. Top views of the initial, transition, and final states for this elementary step on the Cu/Pt surface are shown in Figure 3c−e. We note in passing that, although Cu(111) binds OH(a) + H(a) more strongly than Pt(111) does, the latter appears to break the H−OH bond more easily than the former.The H−OH bond-breaking steps on Cu(111) and on the subsurface alloy Cu/Pt(111) have similar transition state (TS) energies. However, the NSA offers a considerable advantage, namely that the product of the reaction, OH, is bound much more weakly than OH on Cu(111), and therefore the potential for catalyst poisoning by that intermediate is reduced on the Cu/Pt alloy. The activation energy barrier for H_2O activation on Pt(111) is the smallest of those on all three surfaces studied (see Figure 3). Nevertheless, CO poisoning of pure Pt catalysts is the main reason for the low WGS activity observed on those catalysts.

Formate intermediate (HCOO) is another key WGS reaction intermediate known to be rather stable on Cu surfaces.[30] In particular, formate species occupy a large fraction of Cu surface sites under typical WGS conditions, thereby blocking them from participating in active WGS chemistry. Our calculations show that, following the relative binding energy trends established for OH between Cu and Cu/Pt NSA, formate is also destabilized on the Cu/Pt(111) NSA by ca. 0.9 eV at 1/9 ML coverage, compared to its binding on pure Cu(111). This finding suggests that Cu/Pt NSA catalysts should be able to activate H_2O as easily as Cu and, at the same time, be less prone to CO poisoning than pure Pt and more resistant to site blocking by formate than pure Cu surfaces would be.

On the basis of our first-principles calculations, we therefore predict that the reduced poisoning by CO and formate on the Cu/Pt subsurface alloy should make this NSA a very promising and active WGS catalyst. We note here that, as for H_2 dissociation, an NSA is indeed able to activate the H−OH bond

in H_2O relatively easily while binding the products of the reaction rather weakly.[8] Furthermore, the NSAs of Cu/Pt are found to be stable in CO-rich environments, and CO-induced segregation is therefore not expected.[13]

We have thus shown that the stable Cu/Pt NSA is able to activate H_2O (a very common reactant) easily and, at the same time, to bind the products of that reaction and formate intermediates rather weakly, thus avoiding possible poisoning of the catalyst surface. Interestingly, we would like to mention that recently Zhou et al.[32] reported an anomalously high catalytic activity of CuPt core−shell nanoparticles for the NO reduction reaction. After a thorough characterization of their nanoparticles, those authors concluded that the most active phase of their catalysts had Cu preferentially located in the subsurface layers of the Pt nanoparticles.

4. Conclusions

By using a combination of experimental and theoretical model studies, we identified a novel Cu/Pt near-surface alloy which was shown to be a promising candidate for an improved low-temperature WGS catalyst. Such an NSA catalyst might be extremely relevant to hydrogen economy-related catalysis and practice. Advanced nanosynthesis techniques, including electrochemical deposition of metals on metals,[33] dendrimer-based approaches,[34] and atomic layer deposition[35] techniques, all hold a very strong promise for large-scale preparation of NSA catalysts with superior performance when compared to monometallic or bulk alloy catalysts. Such emerging catalyst nanosynthesis techniques can enable the large-scale preparation of improved catalysts, and we hope that the present study will inspire such advances.

Acknowledgment. The authors thank Zheshen Li for his help with the XPS experiments. Work at the University of Wisconsin was supported partly by DOE-BES, Chemical Sciences Division, and partly by grant DE-FG26-06NT42740. We also thank S. C. Johnson & Son, Inc. for a fellowship to A.U.N. Supercomputing time at NERSC, PNNL, and ORNL resources is gratefully acknowledged. J.S. acknowledges financial support by the European Commission through a Marie-Curie Intra-European Fellowship.

JA0700855

(32) Zhou, S. H.; Varughese, B.; Eichhorn, B.; Jackson, G.; McIlwrath, K. *Angew. Chem., Int. Ed.* **2005**, *44*, 4539−4543.
(33) Brankovic, S. R.; Wang, J. X.; Adzic, R. R. *Surf. Sci.* **2001**, *474*, L173−L179.
(34) Ye, H. C.; Crooks, R. M. *J. Am. Chem. Soc.* **2005**, *127*, 4930−4934.
(35) Lim, B. S.; Rahtu, A.; Gordon, R. G. *Nat. Mater.* **2003**, *2*, 749−754.